A Feedback Control Strategy for Energy-Harvesting in Diffusion-Based Molecular Communication Systems

V. Musa, *Student Member, IEEE,* G. Piro, *Member, IEEE,*
L. A. Grieco, *Senior Member, IEEE,* and G. Boggia, *Senior Member, IEEE*

***Abstract*—Piezoelectric nanogenerators recently emerged as a turning point in the design of energy-aware and energy harvesting transmission scheme at the nanoscale. This work considers their adoption in diffusion-based molecular communications, proposing a power control strategy based on feedback control theory. In particular, the transmission power of an electrochemical nanodevice fed by a piezoelectric nanogenerator is dynamically set proportionally to the available energy budget, by using a closed-loop control scheme. The resulting system is analytically modeled with a discrete-time nonlinear state equation. The range of acceptable values of the proportional gain is theoretically derived by studying technological constraints and global asymptotic stability. The impact of the proportional gain on both output variance and time constant of the linearized system around the equilibrium point is also investigated. Computer simulations validate the theoretical analysis under different parameter settings. The comparison against state of the art transmission scheme also demonstrates the unique ability of the conceived approach to ensure, at the equilibrium, the targeted performance level.**

***Index Terms*—Diffusion-based Molecular Communication; Energy Harvesting; System Model; Control Law.**

I. Introduction

The Diffusion-based Molecular Communication (DMC) paradigm promises to enable data exchange among bio-inspired nanodevices [1]. Information messages are encoded with bursts of biochemical particles, which diffuse into the medium without requiring any biological infrastructure [2], [3]. Here, the generation, the release, and the reception of molecules lead to a non-negligible energy consumption [4], [5], but nanodevices can just leverage nano-batteries with limited size and energy capabilities [1]. Therefore, the adoption of energy-aware and energy harvesting techniques plays a key role in DMC systems [3], [6].

The molecule harvesting technique is a possible approach to solve this issue and consists in reusing the molecules retrieved in the past for future communications, thus avoiding to waste energy for the generation of molecules [7]–[11]. Unfortunately, as explicitly highlighted in [11], these contributions only consider the energy cost due to the generation of molecules, while neglecting the amount of energy required to manage the molecules within the nanomachine and the one needed for their release, as well as the actual energy budget available within nanodevices. Other relevant harvesting mechanisms at the nanoscale exploit mechanical and chemical sources [12], [13]. For example, several studies assume to retrieve energy from external vibrations (e.g., the heartbeat in in-vivo applications) through piezoelectric nanogenerators [6], [14]–[17]. The contribution in [6] (by the same authors of this work) investigates, for the first time, the adoption of piezoelectric nanogenerators in DMC systems and conceives a power control mechanism based on feedback control theory. However, it just discusses a very preliminary continuous-time model of the system, which assumes to dynamically tune the number of molecules to transmit for every bit of information, and analyzes asymptotic stability only, without evaluating the impact of the proposed solution on communication performance.

To bridge this gap, this work intends to provide an important step forward in the design of a power control mechanism for DMC systems fed by piezoelectric nanogenerators. In line with the current state of the art, the proposed study models harvesting and discharging processes with an ideal voltage source in series with a resistor and an ultra-nanocapacitor [14] and with a current generator in parallel with the aforementioned ultra-nanocapacitor [6], respectively. Nevertheless, it significantly extends the preliminary formulation presented in [6] in the following directions:

- By assuming the voltage at the ultra-nanocapacitor as the state variable of the system and the resulting energy budget as the feedback variable, the load current (thus, the transmission power) is dynamically tuned through a proportional controller in a closed-loop control scheme and on a per-frame basis. To raise or decrease the transmission power with such a time granularity, the resulting system is analytically modeled with a discrete-time nonlinear state equation, which simultaneously considers harvesting and discharging processes, as well as two independent input parameters (the duty cycle of the signal to transmit and the quantization noise introduced by considering a limited number of load current levels). Once theoretically derived the equilibrium point, some technological constraints are considered to evaluate the acceptable values' range of the proportional gain.
- Non-linear control theory [18] is adopted to demonstrate the global asymptotic stability of the proposed feedback control scheme. The impact of the proportional gain on

The authors are with the Department of Electrical and Information Engineering (DEI), Politecnico di Bari, 70126 Bari, Italy, and also with the Consorzio Nazionale Interuniversitario per le Telecomunicazioni (CNIT), 43124 Parma, Italy. E-mail: {vittoria.musa, giuseppe.piro, alfredo.grieco, gennaro.boggia}@poliba.it.

the variance of the state variable and the time constant of the linearized system around the equilibrium point is determined as well.
- Computer simulations validate all the analytical outcomes and evaluate the performance and the behavior of the communication system under different parameter settings (i.e., by varying the frame size, the communication distance, and the value of the proportional gain).
- Finally, the comparison against state of the art transmission schemes [19], [20] also demonstrates the unique ability of the conceived approach to ensure, at the equilibrium, a Bit Error Rate (BER) lower than the target value of 5%.

The rest of this work is organized as it follows. Section II discusses the state of the art on energy-aware and energy harvesting techniques for micro and nanoscale systems. Section III formulates the reference system model. Section IV describes the conceived closed-loop control scheme and develops its analytical model. Section V discusses numerical and simulation results demonstrating the effectiveness of the proposed approach in conceivable scenarios. Finally, Section VI draws the conclusions and sketches future research activities.

II. State of the Art

In DMC systems, the transmitter releases bursts of molecules by using a specific modulation scheme to encode transmitted bits. According to [3], the On-Off Keying (OOK) represents a very suitable approach for these constrained scenarios: bit 1 is encoded with a burst of molecules and no biochemical entities are released for bit 0 [21], [22]. The reception process is frequently modeled with a reactive receiver implementing the ligand-receptor mechanism: the molecules (namely ligands) reversibly react with a limited number of proteins placed on the receiver surface (namely receptors) and the resulting reception mechanism is described with a second-order reversible reaction. The probability of occurrence of a ligand-receptor reaction depends on the concentration of ligands at the receiver side, the number of receptors, the forward reaction rate constant (i.e., the rate of particle binding with receptors), and the reverse reaction rate constant (i.e., the rate of particle unbinding) [22]–[24]. Finally, signal detection can leverage a sampling-based approach (that compares the number of molecules captured at a given time instant with a threshold value [22]) or an energy-based detection scheme (which makes a decision according to the number of molecules captured during the whole symbol duration [20], [25]). In any case, the communication can be successfully performed only if the transmitter and the receiver implement a synchronization technique, as one of those presented in [26], [27].

The generation, the release, the coding, and the reception of information molecules require a non-negligible amount of energy [4], [5]. Given the limited battery size of nanodevices [3], advanced techniques able to guarantee long-lasting communication capabilities at both micro and nanoscales are, hence, strictly required. Most of the studies on DMC do not take care of any energy constraints [21], [22]. Preliminary energy-aware approaches are presented in [7]–[11]. Differently from the conventional electromagnetic signal, molecules diffuse in the medium without physical attenuation [7]. Hence, received molecules can be stored and reused during subsequent transmission processes [8]. The study in [9] suggests to dynamically adapt transmission settings according to the number of molecules released and captured in the past. The effectiveness of this scheme improves when relay nodes are adopted [10], [11]. Unfortunately, none of the works in [7]–[11] consider all the energy needs related to the communication process and the actual energy budget available within nanodevices, as explicitly highlighted in [11]. Since traditional energy harvesting mechanisms (e.g., solar, thermal, and wind energy harvesting methods) are inefficient in micro and nanoscale scenarios, other solutions have been investigated, based on both mechanical and chemical sources [12], [13]. Chemical and biochemical energies can be harvested by enzymatic fuel cells (namely biofuels) that, once oxidized at the anode side, release electrons. These electrons are driven through an electrical circuit toward the cathode, thus generating electrical energy [28]–[30]. Moreover, mechanical sources can be exploited by means of piezoelectric nanogenerators composed by Zinc Oxide (ZnO) [31]–[36] or lead zirconate titanate [37], [38] nanowires. The vibrations or motions existing in the surrounding environment bent or compress the nanowires generating an electric current at their ends, which charges an ultra-nanocapacitor [39], [40]. Some contributions envisage the adoption of piezoelectric nanogenerators to feed nanodevices willing to communicate through electromagnetic waves at the Terahertz band [14], [15] or to selectively stimulate peripheral nerves in the human body through light signals [16], [17].

For the first time, in [6] a preliminary formulation of a power control mechanism for DMC systems fed by piezoelectric nanogenerators, based on feedback control theory, has been proposed. As anticipated in the Introduction, however, the methodology argued in [6] needs to be further investigated in order to achieve a tractable and effective solution for conceivable scenarios. At the time of this writing and to the best of authors' knowledge, there are not other contributions investigating nor the adoption of piezoelectric nanogenerators in the DMC context, neither the design of advanced transmission scheme leveraging the feedback control theory.

III. System Model at a Glance

The DMC communication system modeled herein includes a point transmitter and a spherical receiver with homogeneously distributed receptors (see Fig. 1).

Transmission model. Transmitter and receiver are supposed to be synchronized, according to one of the mechanisms already proposed in the literature [26], [27]. The transmitter emits N bits long frames by using the OOK modulation. Each bit lasts T_s. The time interval T_b required to release a burst of molecules is much smaller than the symbol duration: $T_b \ll T_s$. By assuming a constant bit rate source, the time interval between the generation of two consecutive frames is defined as $T_f = NT_s + T_i$, where T_i is the idle time between the end of a frame transmission and the beginning of the next

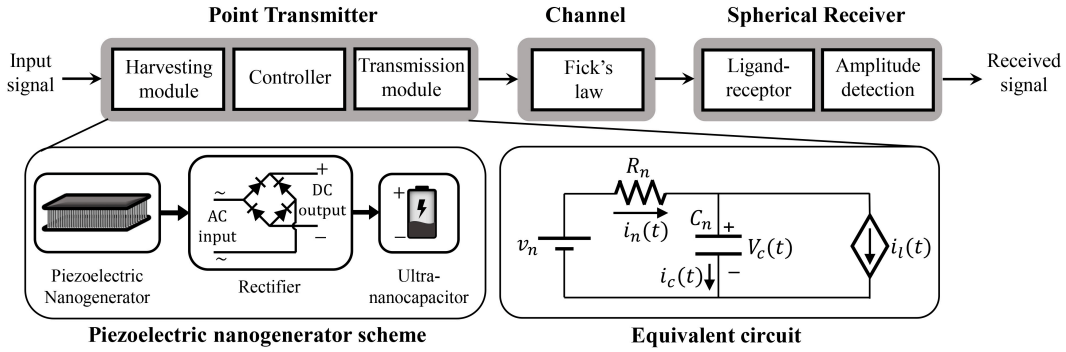

Fig. 1. The considered system model.

frame. Let t_k be the time instant at the beginning of the k-th frame, that is $T_f = t_{k+1} - t_k$. During the k-th frame, a total amount of M_k molecules is released. The duty cycle of the signal to transmit during the k-th frame, $\eta(k)$, it represents the ratio between the amount of time spent to release the bursts of molecules encoding the set of bits 1 in the frame and the total frame duration. Given the occurrence probability of bit 1, ω, its average value and variance are equal to $\bar{\eta} = \omega N T_b/(NT_s+T_i)$ and $\sigma^2_{\tilde{\eta}} = \omega^2 N {T_b}^2/(NT_s + T_i)^2$, respectively.

Propagation model. Released molecules diffuse in a fluid medium according to the Fick's law of diffusion [2]. Therefore, the concentration of molecules at distance d and time t is equal to $c(d,t) = m(4\pi Dt)^{-3/2}\exp(-d^2/4Dt)$, where m is the burst of released molecules and D is the diffusion coefficient. The concentration of molecules reaching the receiver is affected by the diffusion noise and inter-symbol interference [23]. The diffusion noise, $n_d(d,t)$, is due to collisions of information molecules with each other and with the fluid particles in the propagation medium. It can be modeled as an additive white Gaussian noise with zero mean and variance depending on the measured signal. The inter-symbol interference, $n_I(d,t)$, considers the molecular concentration related to the previously transmitted symbols. Indeed, the concentration of molecules that reaches the receiver at distance d and time t is equal to: $c_r(d,t) = c(d,t)+n_d(d,t)+n_I(d,t)$.

Reception model. According to the ligand-receptor reaction [23], the variation of the number of molecules really captured by the receiver, $z_r(d,t)$, is given by $dz_r(d,t)/dt = k_f r c_r(d,t) - k_f c_r(d,t) z_r(d,t) - k_r z_r(d,t)$, where r is the number of receptors, k_f is the forward reaction rate (with a unit of measurement of m^3/s), k_r is the reverse reaction rate (with a unit of measurement of s^{-1}). The signal is sampled in order to detect the maximum number of molecules received in each time slot and it is compared with a given threshold, δ. If the measured signal is higher than the aforementioned threshold, the receiver assumes that the received bit is equal to 1, otherwise the symbol is decoded as 0.

Harvesting and discharging models. The transmitter hosts a piezoelectric nanogenerator, harvesting energy through an array of ZnO nanowires excited by vibrations of the surrounding environment (e.g., the human heartbeat in in-vivo applications) [31]–[36]. The generated alternating current signal is converted into a direct current source by means of a rectifier element. The available energy is finally stored in an ultra-nanocapacitor and consumed during the transmission process [14]–[17]. The equivalent circuit in Fig. 1 models the harvesting and the discharging processes. The harvesting process is modeled through an ideal voltage source, v_n, which generates a current, $i_n(t)$, in series with a resistor, R_n [14]. The voltage generator reproduces the harvesting source providing an amount of electric charge h_n every cycle time of t_n seconds. The value of h_n considers the loss due to the conversion between mechanical and electrical energy [14]. The amount of energy harvested by the surrounding environment is stored in an ultra-nanocapacitor with a capacitance C_n. The voltage across the ultra-nanocapacitor and the current passing through it are denoted with $V_c(t)$ and $i_c(t)$, respectively. The discharging process is modeled with a current source with a load current $i_l(t)$ in parallel with the ultra-nanocapacitor [6]. In this context, the electrical energy stored in the ultra-nanocapacitor is converted into chemical energy through an electrochemical process [41], [42]. Then, the obtained chemical energy is used to generate manage, and release information molecules [4], [5]. The conversion from electrical energy to molecules leads to a further energy loss described by a conversion rate ξ [41], [42]. Considering basic eukaryotic cells as perfect models for bio-inspired nanodevices [5], the amount of energy required to generate and release a burst of molecules is assumed to be comparable with respect to the one consumed by pure biological systems using DMC [4].

The distance between transmitter and receiver and the number of emitted molecules influences the system performance [22]. Specifically, high communication distances can be reached by increasing the number of emitted molecules. Thus, it is necessary to define a lower bound of the number of releasable molecules per bit, m_{min}, that ensures the communication between transmitter and receiver. At the same time, however, a high number of molecules emitted by the transmitter may intensify the impact of inter-symbol interference and diffusion noise, thus impairing the overall communication. Accordingly, an upper bound of the number of releasable molecules per bit, $m_{max} > m_{min}$, is introduced to solve this issue. Given m_{min}, m_{max}, and the frame size, it is possible

TABLE I
LIST OF THE MAIN ANALYTICAL SYMBOLS USED IN THIS WORK.

Communication process
T_f: Time interval between the generation of two consecutive frames; N: Frame size; d: Communication distance; ω: Occurrence probability of bit 1;
Harvesting process
v_n: Generator voltage; R_n: Resistance of circuit modeling the harvesting process; C_n: Capacitance of the ultra-nanocapacitor of circuit modeling the harvesting process; $i_n(t)$: Generator current; $i_c(t)$: Current through the ultra-nanocapacitor; $i_l(t)$: Load current; h_n: Harvested energy per cycle; t_n: Duration of the harvesting cycle.
Control system
$\eta(k)$: Transmission signal duty cycle; $\bar{\eta}$: Average transmission signal duty cycle; $q(k)$: Quantization noise; $\bar{q}$: Average quantization noise; L: Number of quantization levels; Δ_q: Quantization step size; $i_l(k)$: Load current per frame; $V_c(k)$: Voltage across the ultra-nanocapacitor; $E(k)$: Available energy within the ultra-nanocapacitor; $p(k)$: Transmission power per frame; g: Proportional gain of the controller; V_∞: Equilibrium point; ξ: Discharging conversion rate; ϕ_{min}: Minimum frame transmission energy; ϕ_{max}: Maximum frame transmission energy; $e(k)$: Energy consumed for the communication process; $\sigma^2_{V_c}$: Variance of the voltage across the ultra-nanocapacitor; $\sigma^2_{\bar{q}}$: Variance of the quantization noise; $\sigma^2_{\bar{\eta}}$: Variance of the transmission signal duty cycle; τ: Time constant of the linearized system.

to define the minimum (i.e., ϕ_{min}) and the maximum (i.e., ϕ_{max}) amount of energy required to transmit a frame.

IV. THE PROPOSED POWER CONTROL SYSTEM

The proposed power control system is based on the feedback control theory. Table I reports the main analytical symbols used in this work. The devised approach starts considering the equivalent circuit depicted in Fig. 1, analytically described by the Kirchhoff's laws of current and voltage: $v_n = R_n i_n(t) + V_c(t) = R_n i_c(t) + R_n i_l(t) + V_c(t)$. Since the current passing through the ultra-nanocapacitor is derived by the well-known relationship between the voltage across the ultra-nanocapacitor and its current and capacitance, that is $i_c(t) = \dot{V}_c(t) C_n$, the continuous-time process is revised as a linear first-order differential equation:

$$\dot{V}_c(t) = \frac{v_n}{R_n C_n} - \frac{V_c(t)}{R_n C_n} - \frac{i_l(t)}{C_n}. \quad (1)$$

The conceived feedback control scheme intends to raise or decrease the transmission power on a per-frame basis, while keeping it constant during T_f. Under these conditions, a discrete-time model for the control strategy is the natural choice, albeit the controlled plant (i.e., the ultra-nanocapacitor) exhibits a continuous-time dynamic for the discharging and harvesting processes. Accordingly, the control system shown in Fig. 2 embraces an inner continuous-time model (describing the instantaneous discharging process and the harvesting process) and an outer discrete-time model (outlining the per-frame based power control mechanism), while considering the voltage across the ultra-nanocapacitor as the state variable. Let $V_c(k)$ and $i_l(k)$ be the discrete value of both voltage across the ultra-nanocapacitor and load current, respectively, evaluated at the beginning of the k-th frame (i.e., when $t = t_k$). $V_c(k)$ is obtained by sampling the voltage across the ultra-nanocapacitor every T_f. A zero-order hold block is used to convert the discrete value of the load current to its continuous-time representation taken into account by the aforementioned discharging model.

The load current assumes a limited number of levels. Assuming a quantization step size Δ_q, the quantization noise, $q(k)$, can be modeled as a stochastic process with uniform distribution, zero mean, and variance equal to ${\Delta_q}^2/12$. Note that the quantization noise and the duty cycle of the signal to transmit are considered as external inputs to the closed-loop control scheme and are assumed as independent.

The power used to transmit the k-th frame, $p(k)$, is computed by considering the conversion rate ξ, the voltage across the ultra-nanocapacitor at the beginning of the k-th frame, $V_c(k)$, and the resulting load current, $i_l(k)$, while neglecting the amount of energy required to calculate the available energy budget:

$$p(k) = \xi V_c(k) i_l(k). \quad (2)$$

With the aim of ensuring a positive energy consumption during the transmission process, the control law is designed in order to obtain a positive value of $i_l(k)$. To this aim, the proportional gain of the controller, g, can only assume positive values (i.e., $g > 0$); the energy budget available at the ultra-nanocapacitor at the beginning of the k-th frame, $E(k)$, is considered as the feedback variable; and the target point is set to 0 (i.e., $E_0 = 0$). Since $E(k) = C_n {V_c}^2(k)/2$, the resulting closed-loop control scheme is nonlinear.

A. State equation and equilibrium point

The harvesting and discharging processes cause a variation of the amount of energy available in the ultra-nanocapacitor, that can be described through a discrete-time state equation. In fact, the load current is assumed to be constant during the k-th frame, i.e., $i_l(t) = i_l(k)$ in $t_k \leq t \leq t_{k+1}$. Considering an initial condition equal to $V_c(k)$, the solution of eq. (1) is:

$$V_c(t) = \Big(V_c(k) - v_n + i_l(k) R_n\Big) e^{-\frac{1}{R_n C_n}(t - t_k)} + v_n - i_l(k) R_n. \quad (3)$$

Now, by considering $t = t_{k+1}$, after a bit of algebra, the value of the state variable at the beginning of the next frame is:

$$V_c(k+1) = \left(e^{-\frac{t_{k+1} - t_k}{R_n C_n}} - 1\right)(i_l(k) R_n - v_n) + e^{-\frac{t_{k+1} - t_k}{R_n C_n}} V_c(k). \quad (4)$$

The load current $i_l(k)$ is given by the sum of two contributions. The former is proportional to the amount of available energy, $E(k)$, and the duty cycle of the signal to transmit, $\eta(k)$. The latter is the quantization noise $q(k)$. Therefore:

$$i_l(k) = g E(k) \eta(k) + q(k) = g C_n \eta(k) {V_c}^2(k)/2 + q(k). \quad (5)$$

By substituting eq. (5) in (4), it is possible to obtain the state equation of the power control system in Fig. 2:

$$V_c(k+1) = \left(e^{-\frac{T_f}{R_n C_n}} - 1\right)\left[\left(\frac{g C_n \eta(k) {V_c}^2(k)}{2} + q(k)\right) R_n - v_n\right] + e^{-\frac{T_f}{R_n C_n}} V_c(k). \quad (6)$$

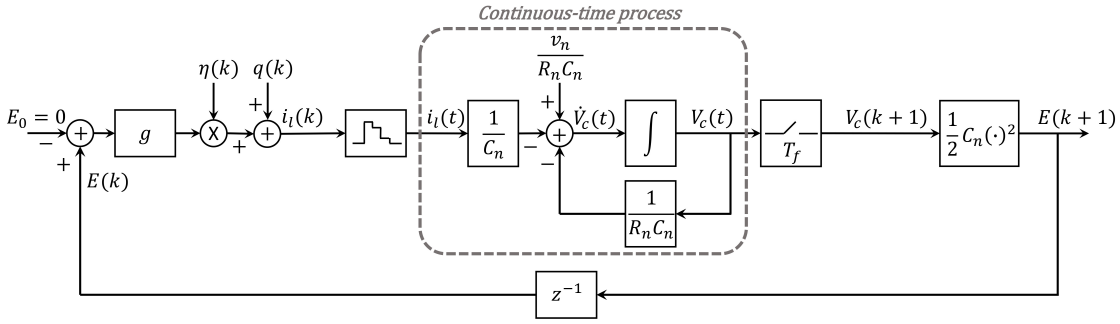

Fig. 2. The conceived closed-loop control scheme.

The state equation captures the behavior of the system over the time. According to the non-linear control theory [18], however, the properties of the resulting nonlinear discrete-time dynamical system, including its stability, can be investigated around its equilibrium point (i.e., the value assumed by the state variable when the system is in a steady-state).

Theorem 1: Due to the nonlinear system modeled in eq. (6), a valid equilibrium point is:

$$V_\infty = (-1 + \sqrt{1 + 4\psi v_n g})/(2\psi g) \tag{7}$$

where $\psi = \bar{\eta} R_n C_n/2$ and $\bar{\eta}$, as defined above, is the average value of the duty cycle, $\eta(k)$.

Proof: The equilibrium points of a discrete-time dynamical system are derived by posing $V_c(k+1) = V_c(k) = V_\infty$ and by assuming constant inputs, that is, the average duty cycle of the signal to transmit, $\eta(k) = \bar{\eta}$, and the mean value of the quantization noise, $q(k) = \bar{q}$. Substituting these values in eq. (6) and considering that the quantization noise is modeled as an uniform noise with zero mean (i.e., $\bar{q} = 0$), the equilibrium points are found by solving a simple second order equation:

$$\begin{aligned} V_\infty = \psi g \left(e^{-\Lambda} - 1\right) {V_\infty}^2 + e^{-\Lambda} V_\infty + \left(1 - e^{-\Lambda}\right)(v_n - R_n \bar{q}) \Rightarrow \\ \Rightarrow \quad g\psi {V_\infty}^2 + V_\infty - v_n = 0. \end{aligned} \tag{8}$$

where $\psi = \bar{\eta} R_n C_n/2$ and $\Lambda = T_f/R_n C_n$ has been introduced to simplify notation.

Now, $V_{\infty 1} = (-1 - \sqrt{1 + 4\psi v_n g})/(2\psi g)$ and $V_{\infty 2} = (-1 + \sqrt{1 + 4\psi v_n g})/(2\psi g)$ are the two roots of Eq. (8). Since the initial assumption on load current requires a positive value of the proportional gain (i.e., $g > 0$), $V_{\infty 1}$ is always negative and it cannot be considered an acceptable equilibrium point. In fact, supposing a negative load current at the equilibrium, the polarization of the voltage across the ultra-nanocapacitor should be inverted and the Kirchhoff's law of the current applied to the equivalent circuit in Fig. 1 implies $i_n(t) = -i_c(t) + i_l(t)$. This means that the load drains more current than the generated one at the equilibrium (i.e., $i_l(t) = i_c(t) + i_n(t) > i_n(t)$), leading to an absurd result. Instead, the second root, $V_{\infty 2}$ provides an acceptable equilibrium point for some values of g, concluding the proof. ■

B. Analysis of the bounds on the proportional gain

Besides the initial assumption on g to guarantee a positive load current (i.e., $g > 0$), other considerations on technological constraints should be done in order to obtain the acceptable range of values of the proportional gain. In fact, it is possible to demonstrate the following result.

Theorem 2: The acceptable range of values of the proportional gain depends on the values of systems parameters as in (9) (see top of the next page).

Proof is reported in the Appendix. It has been derived taking into account that the acceptable values' range for the proportional gain g of the controller jointly requires six conditions: 1) the equilibrium point must be defined in the real domain, 2) the equilibrium point cannot be higher than the source voltage v_n, 3) the amount of energy consumed for communication process at the equilibrium must be higher than the minimum energy consumption level ϕ_{min}, 4) the amount of energy consumed for communication process at the equilibrium must be lower than the maximum energy consumption level ϕ_{max}, 5) the amount of available energy at the equilibrium must be higher than the one required to transmit a frame with N consecutive bits equal to 1, and 6) the voltage across the ultra-nanocapacitor must always be a positive value.

C. Stability analysis

The stability of the proposed discrete-time nonlinear dynamical system is now investigated.

Theorem 3: The equilibrium point in (7), derived in Theorem 1, is globally asymptotically stable for any $g > 0$.

Proof: The global asymptotic stability of the equilibrium point of the discrete-time nonlinear dynamical system described in (6) is evaluated through the Lyapunov's direct method [18]. To this end, a change of variables is introduced to shift the equilibrium point, V_∞, to the origin: $\nu(k) = V_c(k) - V_\infty$. Given that $0 \le V_c(k) \le v_n$, it comes that $-V_\infty \le \nu(k) \le v_n - V_\infty$. The state equation (6) obtained with the constant inputs $\bar{\eta}$ and $\bar{q}$ becomes:

$$\begin{aligned} \nu(k+1) &= f(\nu(k), \bar{\eta}, \bar{q}) = g\psi \left(e^{-\Lambda} - 1\right)(\nu(k) + V_\infty)^2 + \\ &+ e^{-\Lambda}(\nu(k) + V_\infty) + (1 - e^{-\Lambda}) v_n - V_\infty. \end{aligned} \tag{14}$$

The proposed study considers as Lyapunov function $\mathcal{L}(\nu(k)) = \nu^2(k)$, and verifies the following three well-known conditions [18]. First, the Lyapunov function must be positive-definite (i.e., $\mathcal{L}(0) = 0 \wedge \mathcal{L}(\nu(k)) > 0, \forall \nu(k) \neq 0$). This condition is always true because the function is defined as the square of $\nu(k)$. Second, the Lyapunov function must be

$$\begin{cases} \gamma_1 \leq g \leq \gamma_4 & \text{if } (\Psi_b^2 - \Upsilon_b) < 0 \\ \gamma_1 \leq g \leq \gamma_2 \vee \gamma_3 \leq g \leq \gamma_4 & \text{if } (\Psi_b^2 - \Upsilon_b) \geq 0 \quad \text{and} \quad \gamma_1 \leq \gamma_2 \wedge \gamma_3 \leq \gamma_4 \\ \gamma_1 \leq g \leq \gamma_2 & \text{if } (\Psi_b^2 - \Upsilon_b) \geq 0 \quad \text{and} \quad \gamma_1 \leq \gamma_2 \wedge \gamma_3 > \gamma_4 \\ \gamma_3 \leq g \leq \gamma_4 & \text{if } (\Psi_b^2 - \Upsilon_b) \geq 0 \quad \text{and} \quad \gamma_1 > \gamma_2 \wedge \gamma_3 \leq \gamma_4 \\ \nexists g \in \mathbb{R} & \text{if } (\Psi_b^2 - \Upsilon_b) \geq 0 \quad \text{and} \quad \gamma_1 > \gamma_2 \wedge \gamma_3 > \gamma_4 \\ \nexists g \in \mathbb{R} & \text{if } (\Psi_a^2 - \Upsilon_a) < 0 \end{cases} \tag{9}$$

where

$$\gamma_1 = \frac{-\Psi_a - \sqrt{\Psi_a^2 - \Upsilon_a}}{{\phi_{min}}^2 \chi}; \qquad \gamma_2 = \frac{-\Psi_b - \sqrt{\Psi_b^2 - \Upsilon_b}}{{\phi_{max}}^2 \chi}; \qquad \gamma_3 = \frac{-\Psi_b + \sqrt{\Psi_b^2 - \Upsilon_b}}{{\phi_{max}}^2 \chi} \tag{10}$$

$$\gamma_4 = \min\left(\frac{-\Psi_a + \sqrt{\Psi_a^2 - \Upsilon_a}}{{\phi_{min}}^2 \chi}, \frac{C_n R_n + 2T_f}{8\bar{\eta} v_n {T_f}^2}, \frac{4LT_s}{R_n C_n v_n T_b \left(1 - e^{-\Lambda}\right)(2L+1)} \right) \tag{11}$$

$$\Psi_a = v_n \xi T_f (3\phi_{min} R_n - {v_n}^2 \xi T_f); \qquad \Upsilon_a = 4{\phi_{min}}^3 \xi T_f {R_n}^3; \qquad \chi = \bar{\eta} C_n {R_n}^3 \tag{12}$$

$$\Psi_b = v_n \xi T_f (3\phi_{max} R_n - {v_n}^2 \xi T_f); \qquad \Upsilon_b = 4{\phi_{max}}^3 \xi T_f {R_n}^3. \tag{13}$$

radially unbounded (i.e., $|\nu(k)| \to \infty \Rightarrow \mathcal{L}(\nu(k)) \to \infty$). Also in this case, it is always satisfied and the related proof is trivial. Third, the derivative of the Lyapunov function, calculated with respect to the variable $\nu(k)$, must be negative-definite (i.e., $\dot{\mathcal{L}}(0) = 0 \wedge \dot{\mathcal{L}}(\nu(k)) < 0, \forall \nu(k) \neq 0$). In particular, $\dot{\mathcal{L}}(\nu(k))$ can be computed as: $\dot{\mathcal{L}}(\nu(k)) = \mathcal{L}(\nu(k+1)) - \mathcal{L}(\nu(k))$. Thus, considering eq. (14):

$$\begin{aligned} \dot{\mathcal{L}}(\nu(k)) &= \mathcal{L}(\nu(k+1)) - \mathcal{L}(\nu(k)) = \\ &= \mathcal{L}(f(\nu(k), \bar{\eta}, \bar{q})) - \mathcal{L}(\nu(k)) = \\ &= \left[g\psi(e^{-\Lambda} - 1)(\nu(k) + V_\infty)^2 + e^{-\Lambda}(\nu(k) + V_\infty) + \right. \\ &+ \left. (1 - e^{-\Lambda}) v_n - V_\infty \right]^2 - \nu^2(k). \end{aligned} \tag{15}$$

Numerically, it is possible to note that the (15) is equal to zero only when $\nu(k) = 0$, otherwise it always assumes negative values. Thus, this third condition is satisfied for any value of g. ∎

It is possible to conclude that the acceptable values' range of the proportional gain g given by Theorem 2 always makes the equilibrium point V_∞ globally asymptotically stable. Accordingly, the dynamical system modeled in (6) will converge to the equilibrium point for any initial condition (i.e., for any $V_c(0) \in [0, v_n]$) as the time index k is large enough.

D. Impact of the proportional gain on both output variance and time constant

The variation of the voltage across the ultra-nanocapacitor is surely influenced by the dynamics of system inputs. However, the choice of the proportional gain has a clear impact on the variance of the output. Defining $\widetilde{V}_c(k) = V_c(k) - V_\infty$, $\widetilde{V}_c(k+1) = V_c(k+1) - V_\infty$, $\widetilde{\eta}(k) = \eta(k) - \bar{\eta}$, and $\widetilde{q}(k) = q(k) - \bar{q}$, the following result states.

Theorem 4: Considering the linearized system around the equilibrium point, the variance of the duty cycle, $\sigma_{\widetilde{\eta}}^2$, and the variance of the quantization noise, $\sigma_{\widetilde{q}}^2$, the variance of the output, $\sigma_{\widetilde{V}_c}^2$, is equal to:

$$\sigma_{\widetilde{V}_c}^2 = \left(\alpha_2^2 \sigma_{\widetilde{\eta}}^2 + \alpha_3^2 \sigma_{\widetilde{q}}^2\right) / (1 - \alpha_1^2). \tag{16}$$

where $\alpha_1 = 2g\psi\left(e^{-\Lambda} - 1\right) V_\infty + e^{-\Lambda}$; $\alpha_2 = \frac{g\psi}{\bar{\eta}} {V_\infty}^2 \left(e^{-\Lambda} - 1\right)$; $\alpha_3 = R_n \left(e^{-\Lambda} - 1\right)$.

Proof: The discrete-time nonlinear dynamical system in eq. (6) and reported in what follows as $V_c(k+1) = f(V_c(k), \eta(k), q(k))$, can be approximated with its linearization around the equilibrium point by means of the Taylor series when the time index k is large enough:

$$\begin{aligned} V_c(k+1) &= f(V_c(k), \eta(k), q(k)) \approx \\ &\approx f(V_\infty, \bar{\eta}, \bar{q}) + \nabla f(V_\infty, \bar{\eta}, \bar{q}) \cdot \left[\widetilde{V}_c(k) \ \widetilde{\eta}(k) \ \widetilde{q}(k) \right]^T. \end{aligned} \tag{17}$$

By definition, $f(V_\infty, \bar{\eta}, \bar{q}) = V_\infty$. Considering the variable $\widetilde{V}_c(k+1)$, the linearized state equation becomes:

$$\begin{aligned} \widetilde{V}_c(k+1) &= \left. \frac{\partial f(V_c(k), \eta(k), q(k))}{\partial V_c(k)} \right|_{V_\infty, \bar{\eta}, \bar{q}} \widetilde{V}_c(k) + \\ &+ \left. \frac{\partial f(V_c(k), \eta(k), q(k))}{\partial \eta(k)} \right|_{V_\infty, \bar{\eta}, \bar{q}} \widetilde{\eta}(k) + \\ &+ \left. \frac{\partial f(V_c(k), \eta(k), q(k))}{\partial q(k)} \right|_{V_\infty, \bar{\eta}, \bar{q}} \widetilde{q}(k) = \\ &= \left(2g\psi\left(e^{-\Lambda} - 1\right) V_\infty + e^{-\Lambda}\right) \widetilde{V}_c(k) + \\ &+ \left(\frac{g\psi}{\bar{\eta}} {V_\infty}^2 \left(e^{-\Lambda} - 1\right) \right) \widetilde{\eta}(k) + \\ &+ \left(R_n \left(e^{-\Lambda} - 1\right)\right) \widetilde{q}(k) = \\ &= \alpha_1 \widetilde{V}_c(k) + \alpha_2 \widetilde{\eta}(k) + \alpha_3 \widetilde{q}(k). \end{aligned} \tag{18}$$

Starting from eq. (18) and remembering that the external inputs are independent, it is possible to evaluate the variance of the state variable, $\sigma_{\widetilde{V}_c}^2$, as a function of the variance of input variables, $\sigma_{\widetilde{\eta}}^2$ and $\sigma_{\widetilde{q}}^2$, that is: $\sigma_{\widetilde{V}_c}^2 = \alpha_1^2 \sigma_{\widetilde{V}_c}^2 + \alpha_2^2 \sigma_{\widetilde{\eta}}^2 + \alpha_3^2 \sigma_{\widetilde{q}}^2 \Rightarrow \sigma_{\widetilde{V}_c}^2 = \left(\alpha_2^2 \sigma_{\widetilde{\eta}}^2 + \alpha_3^2 \sigma_{\widetilde{q}}^2\right) / (1 - \alpha_1^2)$. ∎

Now, it is possible to evaluate the time constant of the linearized system around the equilibrium point, τ, to understand how fast the system returns at the equilibrium after a perturbation of the external inputs. In particular, the following result holds.

Theorem 5: The time constant of the linearized system around the equilibrium point is:

$$\tau = -T_f \Big/ \ln\left(1 - \left(1 - e^{-\Lambda}\right)\sqrt{1 + 4\psi v_n g}\right). \quad (19)$$

Proof: Considering the linearized discrete-time dynamical system reported in (18), its z-transform is $z\mathcal{V}_c(z) = \alpha_1\mathcal{V}_c(z) + \alpha_2\mathcal{H}(z) + \alpha_3\mathcal{Q}(z)$, where $\mathcal{V}_c$, $\mathcal{H}$ and $\mathcal{Q}$ are the z-transform of $\widetilde{V_c}$, $\widetilde{\eta}$ and $\widetilde{q}$, respectively. Due to the linearity of the dynamical system, it is possible to analyze separately the two inputs by the superposition principle. Thus, the transfer function depending on the duty cycle of the signal to transmit is $\mathcal{V}_c(z)/\mathcal{H}(z) = \alpha_2/(z - \alpha_1)$. At the same time, the transfer function of the dynamical system depending only on the quantization noise is: $\mathcal{V}_c(z)/\mathcal{Q}(z) = \alpha_3/(z - \alpha_1)$. The pole of the transfer function is equal to α_1 in both cases. Thus, considering the relationship between the z-plane and the s-plane (i.e., $z = e^{sT_f}$) and the relationship between the pole and the time constant in continuous-time first order system (i.e., $s = -1/\tau$), the time constant of the linearized system around the equilibrium point is computed starting from the pole in the z-plane, that is: $z = \alpha_1 = e^{-\frac{T_f}{\tau}}$. Accordingly, given $\tau = -T_f/\ln(\alpha_1)$ and (18), the proof is concluded. ■

The partial derivative of (19) with respect to the proportional gain g is reported in (20) (see top of the next page).

Since its sign is negative, it comes that a bigger value of proportional gain is preferred to obtain a smaller time constant of the linearized system and, in turn, a faster response of the system at the equilibrium. On the other hand, Theorem 4 demonstrates that smaller values of the proportional gain g usually involve smaller variance of the output. Hence, the choice of the suitable g must be the result of a trade-off between these two conditions.

E. Discussion on implementation and computational complexity

The scientific literature on nanotechnology remarks that the realization of computing, storing, and communication elements of a nanomachine is now feasible [3], bio-inspired machines communicating via molecular diffusion have been already realized in macroscale experimental testbeds [43], stand-up ZnO nanowires can be used to create ultra-nanocapacitor feeding nano-devices [39], [40], and proportional controller [44] and uniform quantizers [45] can be implemented at the nanoscale. Thus, the practical implementation of the presented power control mechanism in the near future requires a deep integration process, which fully reflects the interests of both research and industry working in this application domain.

The proposed scheme assumes that parameter settings (i.e., information related to the physical layer, application layer, and harvesting circuit) and deployment details (i.e., the distance between transmitter and receiver and the diffusion coefficient of the medium) are known a priori. Indeed, they can be used to properly set the value of the proportional gain of the controller, without requiring any further signaling overhead. The power transmission is calculated, for each frame, through four multiplications: $p(k) = (0.5\xi C_n g) \cdot \eta(k) \cdot V_c(k) \cdot V_c(k) \cdot V_c(k)$. Since the computational complexity does not depend on system parameters and is the same for each frame, it can be considered as a constant, that is $O(1)$.

V. Performance evaluation

The behavior of the proposed approach in conceivable scenarios and the goodness of the formulated theoretical analysis is evaluated through Matlab scripts, modeling the communication system described in Section III and the control law formulated in Section IV. Most of the system parameters are set according to the current scientific literature: the distance between transmitter and receiver is chosen in the range from 1 μm to 30 μm [22], the diffusion coefficient of the aqueous medium is set to $D = 10^{-9}$ m^2/s [24], symbol duration and burst duration are set to $T_s = 1$ s and $T_b = 1$ ms, respectively [22], the target BER is set to 5%. Considering an ultra-nanocapacitor based on onion-like carbon electrodes, conceivable values for the charge generated per unit area in each cycle time and the capacitance per unit area are 6 fC/μm^2 [15], [33] and 9 pF/μm^2 [15], [40], respectively. As 1000 μm^2 is a conceivable size of both piezoelectric nanogenerator and ultra-nanocapacitor, the amount of charge per cycle, h_n, and the capacitance of the ultra-nanocapacitor, C_n, are set to 6 pC and 9 nF, respectively [15], [40]. A conceivable value for the generator voltage is 0.42 V [14], [15], [37]. The resulting source resistor is $R_n = v_n t_n / h_n$, where the time duration of the harvesting cycle is set to $t_n = 1$ s [14].

To validate analytical models discussed in Section IV, conducted tests consider the transmission of adjacent frames (i.e., the worst condition, where $T_i = 0$) for 2000 s. The frame size is set from 10 to 30 bits. Assuming equiprobable bits ($\omega = 0.5$) [22], the average duty cycle is: $\bar{\eta} = \omega T_b / T_s = 5 \cdot 10^{-4}$. The electrical energy stored within the ultra-nanocapacitor is supposed to be converted into chemical energy through the water electrolysis process, which has a conversion rate equal to 40% [41]. The resulting chemical energy is adopted to generate insulin molecules through the polymerization of amino acids and release them, as for pure biological systems [4]. The quantization is modeled by considering the number of quantization levels, L, equal to 2^8. With reference to the reception process, the ligand-receptor reaction and the amplitude detection scheme are used to decode the transmitted signal. The number of receptors r, the forward reaction rate constant k_f, and the reverse reaction rate constant k_r are set to 500, 20 μm^3/s, and 30 s^{-1}, respectively [23] [24]. Concerning the detection process, the threshold δ is set to the half of the maximum number of molecules received during the symbol duration at the equilibrium. Finally, to reduce the effect of statistical fluctuations, results have been obtained by averaging 1000 independent simulations.

A. Transmission requirements

Matlab scripts are used to model the communication system described in Section III, while considering the transmission of several consecutive frames, different communication distances, and different number of molecules encoding the bit 1. The minimum amount of energy required to transmit a frame,

$$\frac{\partial \tau}{\partial g} = -\frac{2\psi v_n T_f \left(1 - e^{-\Lambda}\right)}{\sqrt{1+4\psi v_n g}\left(1-\left(1-e^{-\Lambda}\right)\sqrt{1+4\psi v_n g}\right)\ln^2\left[1-\left(1-e^{-\Lambda}\right)\sqrt{1+4\psi v_n g}\right]} < 0. \quad (20)$$

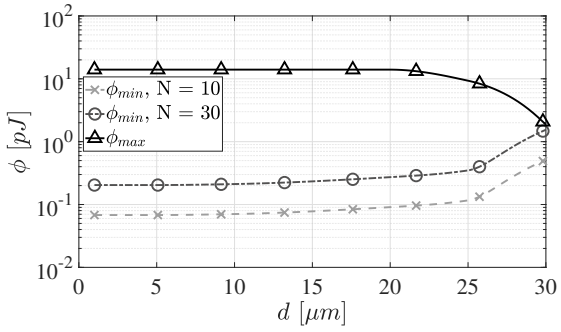

Fig. 3. Minimum and maximum amount of energy required to transmit a frame.

ϕ_{min}, is computed by assuming to uniformly distribute the related number of molecules across $N/2$ bits equal to 1 (i.e., $\omega = 0.5$). For each communication distance, tests identified the minimum number of molecules released for the transmission of bit 1, m_{min}, and in turn the value of ϕ_{min}, that ensures an average BER lower than 5%. Similarly, the maximum amount of energy required to transmit a frame, ϕ_{max}, is computed by considering frames with only one bit per frame equal to 1 (the whole transmission power is used for emitting only one bit, thus generating the highest diffusion noise and inter-symbol interference). Results reported in Fig. 3 show that ϕ_{min} increases with the frame size and the communication distance. In fact, given that ϕ_{min} is dimensioned for transmitting $N/2$ bits equal to 1, the higher the frame size, the higher the number of molecules released for each frame. Moreover, when the communication distance increases, the concentration of molecules that reaches the receiver sphere decreases. Thus, in order to guarantee a given target BER, higher communication distances require more emitted molecules. On the other hand, ϕ_{max} decreases when the communication distance increases. In fact, according to the Fick's law of diffusion, some of the molecules emitted for a given symbol remain around the receiver sphere also after the related symbol duration, thus generating diffusion noise and inter-symbol interference. The impact of these noise contributions is not negligible when the communication distance increases, affects the detection process and impairs the communication performance. This effect increases with the number of emitted molecules. Furthermore, when the communication distance is higher than $d = 30$ μm, the value of the minimum required energy ϕ_{min} becomes greater than the value of the maximum required energy ϕ_{max} for $N = 30$. Therefore, the constraints presented in Theorem 2 cannot be satisfied and the system is unfeasible.

B. Equilibrium point vs acceptable values of the proportional gain

By considering Theorem 2, Fig. 4 depicts the equilibrium point, V_∞, as a function of the acceptable values of the proportional gain. Note that the acceptable values' range of g reduces with the frame size and the communication distance. The extreme case is registered when $N = 30$ and $d = 30$ μm. The value of the equilibrium point decreases when the proportional gain increases. In fact, higher values of g lead to an increment of the resulting energy budget consumed for the transmission. This, in turn, implies a reduction of the resulting energy budget at the equilibrium. The rest of this Section considers two different examples of the proportional gain, corresponding to a low and a high value extracted from the acceptable range (see Table II).

C. Analysis of the state variable at the equilibrium

The time variation of the state variable is reported in Fig. 5. As already explained, a higher value of proportional gain g corresponds to a lower equilibrium point, reached after a lower amount of time. Nevertheless, given the global asymptotic stability of the equilibrium point, the expected theoretical value of V_∞ is always reached. When $N = 10$, the communication distance does not influence the results because the range of acceptable values of g (and, hence, those selected for the numerical study) is almost the same. A different behavior is registered when $N = 30$. In any case, it is important to note that the higher the communication distance, the higher the energy budget at the equilibrium. This result is not surprising: as discussed in Section V-B, a high communication distance only accepts a limited set of lower values of g. Accordingly, the amount of energy consumed during the transmission process is limited, and the resulting energy budget stored into the ultra-nanocapacitor growths.

D. Energy consumption and achieved performance

The amount of energy consumed during the time is reported in Fig. 6. The highest energy consumption is registered when the high value of g is considered, while a smaller proportional gain corresponds to a lower energy consumption. When $N = 10$, the differences between the amount of energy consumed for different communication distances are negligible because the range of acceptable g is approximately the same. On the contrary, differences can be observed when $N = 30$. Also in this case, a lower amount of energy is consumed when the communication distance increases because of the selected values of the proportional gain.

Fig. 7 depicts the achieved communication performance. The behavior of the proposed approach is compared against traditional communication schemes encoding the symbol 1 through a burst of a constant number of molecules. Without loss of generality, the study considers static transmission scheme where $m = 100$ (a very little value suggested in [19]) and $m = 20000$ (a larger value proposed in [20]). The proposed power control mechanism registers an average BER very closed to 50% just at the beginning of the transmission

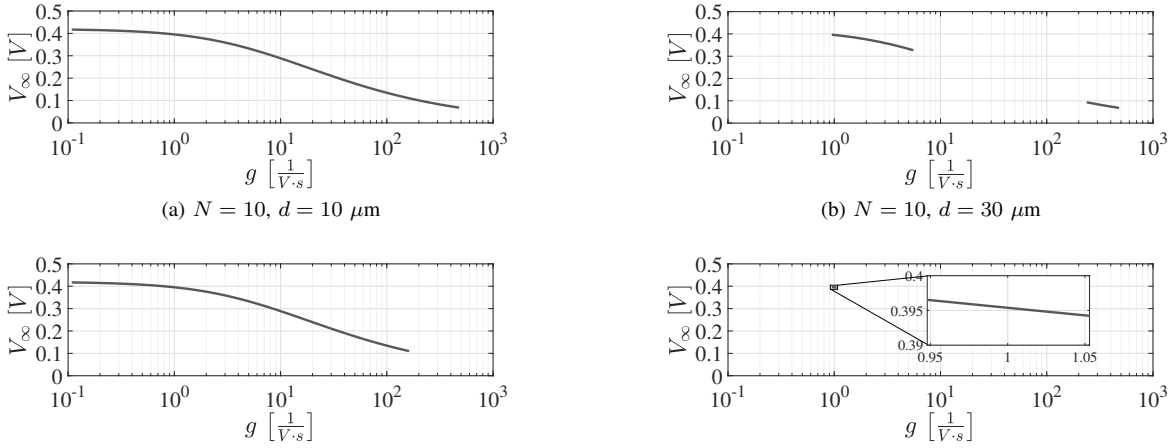

(a) $N = 10$, $d = 10$ μm (b) $N = 10$, $d = 30$ μm

(c) $N = 30$, $d = 10$ μm (d) $N = 30$, $d = 30$ μm

Fig. 4. Equilibrium point, V_∞, as a function of the proportional gain g.

TABLE II
LIST OF PROPORTIONAL GAIN VALUES USED IN THE PERFORMANCE EVALUATION

	$N = 10$		$N = 30$	
	$d = 10$ μm	$d = 30$ μm	$d = 10$ μm	$d = 30$ μm
γ_{low} (low proportional gain) [$V^{-1}s^{-1}$]	5	5	5	0.95
γ_{high} (high proportional gain) [$V^{-1}s^{-1}$]	479.04	479.04	162.22	1.05

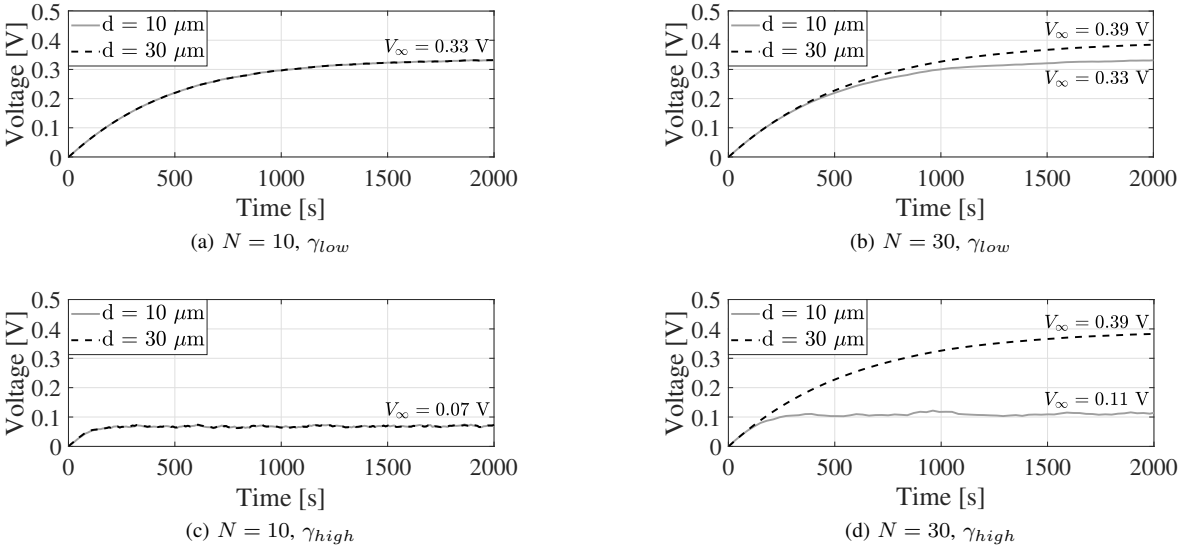

(a) $N = 10$, γ_{low} (b) $N = 30$, γ_{low}

(c) $N = 10$, γ_{high} (d) $N = 30$, γ_{high}

Fig. 5. The state variable, $V_c(k)$, as a function of the time.

process, because the ultra-nanocapacitor is empty and the state variable is very far from its equilibrium point. When the system approaches the equilibrium, the performance sharply improves and the measured BER goes below the target value. A higher communication distance generally implies a higher BER, because of the reduced number of molecules reaching the receiver and the high impact of both diffusion noise and inter-symbol interference. The amount of time needed by the system to reach the equilibrium point increases when the value of the proportional gain decreases. On the other hand, traditional transmission schemes are able to guarantee the target performance level only when the number of emitted molecules and the communication distance are very low (i.e., $m = 100$ and $d = 10$ μm). In the other cases, most of the time the transmission process fails (i.e., the receiver does not receive any molecules and decodes all the bits of the frame as 0-bits) because of the limited, or at most absent, energy budget. As a result, the comparison against state of the art transmission scheme clearly demonstrates the unique ability of the conceived approach to ensure, at the equilibrium, the expected target BER.

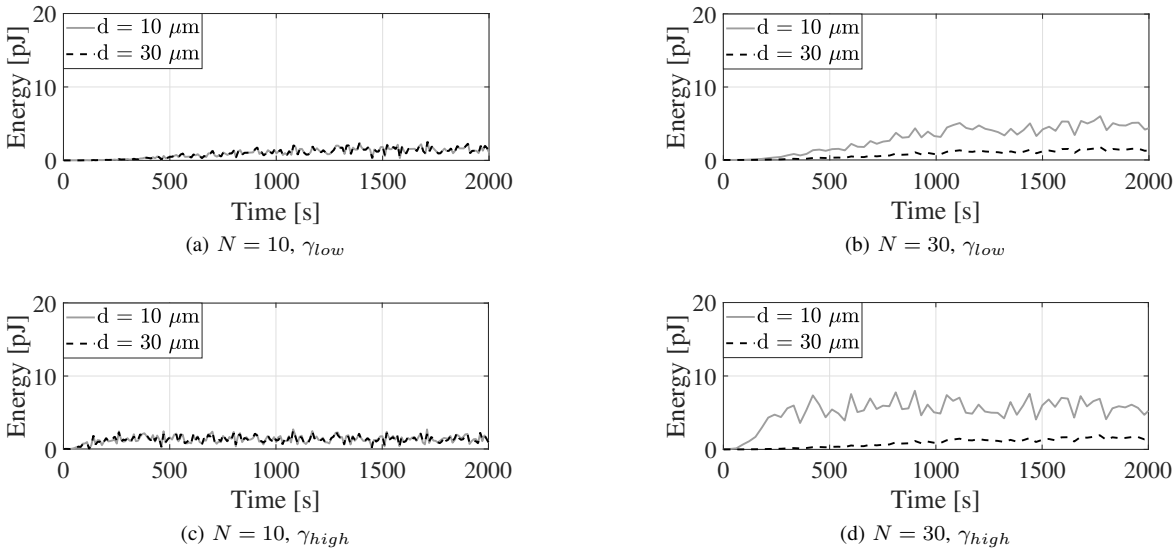

(a) $N = 10$, γ_{low} (b) $N = 30$, γ_{low}

(c) $N = 10$, γ_{high} (d) $N = 30$, γ_{high}

Fig. 6. The consumed energy as a function of the time.

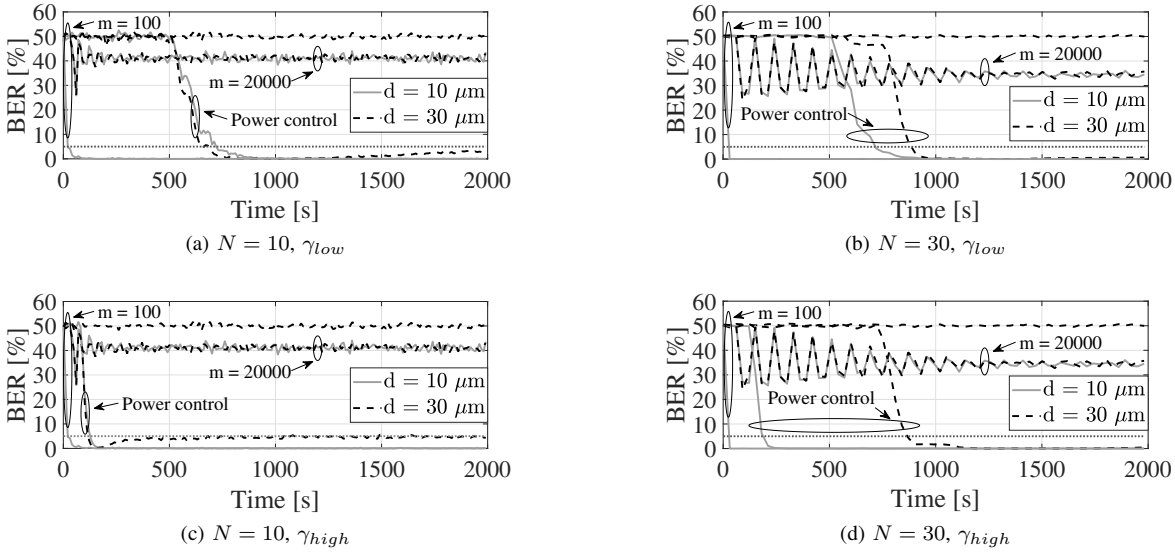

(a) $N = 10$, γ_{low} (b) $N = 30$, γ_{low}

(c) $N = 10$, γ_{high} (d) $N = 30$, γ_{high}

Fig. 7. The average BER as a function of the time. The dotted line represents the target BER of 5%.

E. Impact of the duty cycle on both variance of the output and time constant

To evaluate the variance of the state variable (that represents the output of the modeled system) as a function of the variance of the inputs, the duty cycle of the signal to transmit is changed by setting the idle time T_i from 0 s to 10 s (see Fig. 8). First of all, computer simulations confirm the goodness of the formulated analytical model (specifically, Theorem 4). Moreover, it is possible to observe that when $d = 10$ μm, the higher the T_i (hence, the lower the duty cycle), the higher the variance of the output. In this case, the choice of a lower value of acceptable proportional gains also ensures a lower variability of the state variable. On the other hand, larger communication distances further decrease the variance of the output.

Finally, the time constant is investigated to evaluate the time required by the linearized system to return at the equilibrium after a perturbation of input parameters. Assuming that the system is at the equilibrium (i.e., the amount of energy available within the ultra-nanocapacitor is equal to the energy budget at the equilibrium), an input perturbation is modeled by considering that a certain number of frames entirely composed by 1-bits should be transmitted by the nano-device. This perturbation leads to a decrement of the available energy in the ultra-nanocapacitor, thus reducing the value of the state variable. Starting from Fig. 9, it is possible to demonstrate that, when the duty cycle of the signal to transmit returns to its average value, the time required by the system to reach the 95% of its equilibrium point is equal to three-times the time constant computed for the linearized system in Theorem 5. At the same time, it is possible to note that a lower proportional gain determines a larger time constant of the

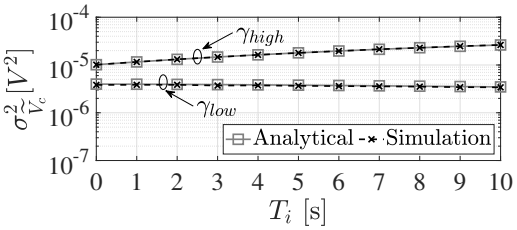

(a) $N = 10$, $d = 10$ μm

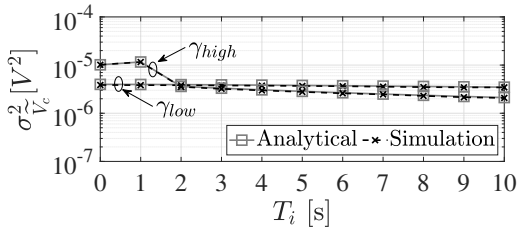

(b) $N = 10$, $d = 30$ μm

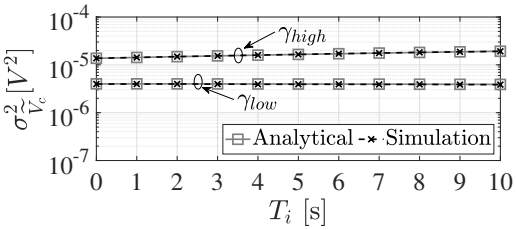

(c) $N = 30$, $d = 10$ μm

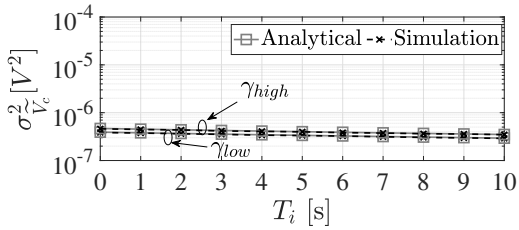

(d) $N = 30$, $d = 30$ μm

Fig. 8. The variance of the output, $\sigma^2_{\widetilde{V_c}}$, as a function of the idle time, T_i.

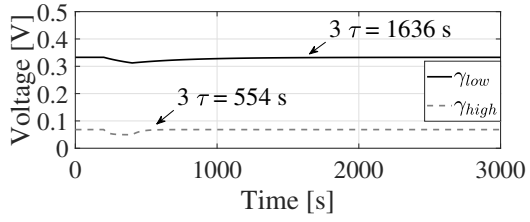

(a) $N = 10$, $d = 10$ μm

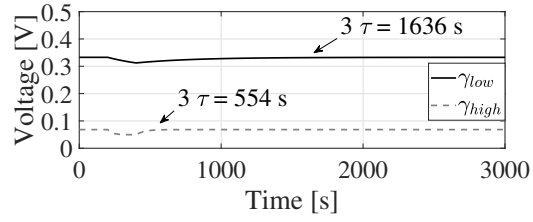

(b) $N = 10$, $d = 30$ μm

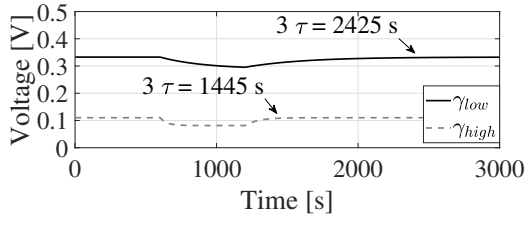

(c) $N = 30$, $d = 10$ μm

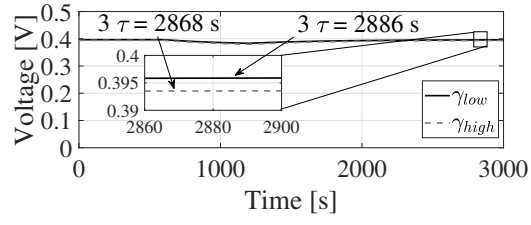

(d) $N = 30$, $d = 30$ μm

Fig. 9. The average state variable as a function of the time when a perturbation of the inputs occurs.

linearized system around the equilibrium point. The frame size and the communication distance influence the time constant of the linearized system as well: the extreme case (i.e., $d = 30$ μm and $N = 30$) corresponds to a restricted range of lower acceptable g and, in turn, implies a slower system.

VI. Conclusion

This work presented a power control mechanism exploiting the feedback control theory, whose goal is to guarantee a long-lasting diffusion-based molecular communication between electrochemical nano-devices fed by a piezoelectric nanogenerator. The resulting system has been modeled with a discrete-time nonlinear state equation and deeply studied to evaluate acceptable settings guaranteeing technological constraints and global asymptotic stability. Computer simulations validated all the presented analytical models. Obtained results also demonstrated that higher values of the proportional gain bring to lower equilibrium points, the state variable always tends to the theoretical equilibrium point, the conceived communication system always ensures a BER lower than the target value when an acceptable value of the proportional gain is chosen, the variance of the output is strongly affected by the variance of the inputs and the proportional gain, and the time required by the system to return at the equilibrium after a perturbation of the inputs decreases with the increment of the proportional gain. The comparison against state of the art transmission scheme further demonstrated the unique ability of the conceived approach to ensure, at the equilibrium, the expected performance level. Future research activities will also explore the reception procedure, multiple communications, more sophisticated transmission techniques, and variable system requirements.

$$\frac{\partial f(V_c(k),\eta(k),q(k))}{\partial \eta(k)} = -\frac{2e^{-\Lambda}V_c(k) + 2(1-e^{-\Lambda})\left(v_n - q(k)R_n\right)}{C_n R_n (1-e^{-\Lambda}) {V_c}^2(k)\eta^2(k)} < 0,$$
$$\frac{\partial f(V_c(k),\eta(k),q(k))}{\partial q(k)} = -\frac{2}{C_n \eta(k) {V_c}^2(k)} < 0,$$
$$\frac{\partial f(V_c(k),\eta(k),q(k))}{\partial V_c(k)} = -\frac{2e^{-\Lambda}V_c(k) + 4\left(1-e^{-\Lambda}\right)\left(v_n - q(k)R_n\right)}{\eta(k) C_n R_n (1-e^{-\Lambda}) {V_c}^3(k)} < 0. \quad (21)$$

APPENDIX

Herein, the proof of Theorem 2 is reported. The acceptable range of values of the proportional gain depends on the values of systems parameters and it is achieved by jointly considering the following six conditions.

The first condition refers to the study of the domain of the equilibrium point function in eq. (8), according to which the argument of the squared root must be positive and the denominator cannot assume zeros values: $1 + 4\psi v_n g \geq 0$ and $2\psi g \neq 0$. Analytically, this condition is verified if $g \geq -1/4\psi v_n$ and $g \neq 0$, respectively. Therefore, considering the initial assumption on the proportional gain of the controller (i.e., $g > 0$), this first condition is always satisfied.

The second condition deals with the upper bound of the voltage across the ultra-nanocapacitor, equal to the voltage provides by the generator, v_n. The voltage at the equilibrium cannot exceed the source voltage, v_n, that is $V_\infty \leq v_n$. Analytically, by considering (7), this condition becomes: $V_\infty = (-1 + \sqrt{1 + 4\psi v_n g})/2\psi g \leq v_n$ which is only verified for $g > 0$. Also in this case, considering the initial assumption on the proportional gain, this condition is always satisfied.

The third condition focuses on the value of the load current $i_l(k)$ provided by the closed-loop control scheme at the equilibrium. As already argued in Section III, the amount of energy consumed for communication process at the equilibrium, $e(k)|_{V_\infty,\bar{\eta},\bar{q}}$, should ensure the transmission of the minimum number of molecules that guarantees the desired level of performance: $e(k)|_{V_\infty,\bar{\eta},\bar{q}} = p(k)T_f|_{V_\infty,\bar{\eta},\bar{q}} \geq \phi_{min}$. Indeed, given (2) and (5), the third condition can be expressed as: $e(k)|_{V_\infty,\bar{\eta},\bar{q}} = \xi C_n \bar{\eta} T_f g {V_\infty}^3/2 \geq \phi_{min}$. Analytically, it is verified if $\gamma_1 \leq g \leq (-\Psi_a + \sqrt{\Psi_a^2 - \Upsilon_a})/(\phi_{min}{}^2 \chi)$, where parameters have been defined in (10)-(13). This inequality influences the value of γ_4 in the Theorem and the maximum considerable value for the minimum energy per frame, ϕ_{min}, by posing the argument of the squared root as $\Psi_a^2 - \Upsilon_a \geq 0$. This constraint is verified if $\phi_{min} \leq {v_n}^2 \xi T_f/4R_n$. Otherwise the entire system is unfeasible.

The fourth condition considers that an excessive number of transmitted molecules drastically impairs the communication performance, as highlighted in Section III. Thus, the energy consumption associated with the closed-loop control scheme should not be higher than the one needed to transmit the maximum number of molecules guaranteeing the target performance: $e(k)|_{V_\infty,\bar{\eta},\bar{q}} = p(k)T_f|_{V_\infty,\bar{\eta},\bar{q}} \leq \phi_{max}$. Starting from (2) and (5), the fourth condition states that: $e(k)|_{V_\infty,\bar{\eta},\bar{q}} = \xi C_n \bar{\eta} T_f g {V_\infty}^3/2 \leq \phi_{max}$. This condition is always verified if $\Psi_b^2 - \Upsilon_b < 0$. Otherwise, it is satisfied only if $g \leq \gamma_2$ or $g \geq \gamma_3$. Considering the initial assumption on the proportional gain (i.e., $g > 0$), the solution of the fourth condition is $0 \leq g \leq \gamma_2$ or $g \geq \gamma_3$.

The fifth condition assumes that the system should have, at the equilibrium, an amount of energy greater than the one needed to transmit a frame with N consecutive bits equal to 1, that is: ${C_n V_\infty}^2/2 \geq g C_n T_f \bar{\eta} {V_\infty}^3$. Analytically, it is satisfied if $g \leq (C_n R_n + 2T_f)/8\bar{\eta} v_n {T_f}^2$ and $g \neq 0$. Considering the initial assumption on the proportional gain of the controller (i.e., $g > 0$), the fifth condition is verified if $0 < g \leq (C_n R_n + 2T_f)/8\bar{\eta} v_n {T_f}^2$. This constraint is useful for the calculation of γ_4 used in the Theorem.

The sixth condition states that the voltage across the ultra-nanocapacitor must always be a positive value to avoid changing of polarization: $V_c(k) \geq 0$ for all $k \in \mathbb{N}$. This is verified by means of the principle of induction. Starting from $V_c(0) = V_0 \geq 0$ and supposing that $V_c(k) \geq 0$ is true, it is possible to compute the values of g respecting the sixth condition by imposing $V_c(k+1) \geq 0$. Considering the state equation (6), the following inequality is introduced:

$$g \leq \frac{2e^{-\Lambda}V_c(k) + 2\left(1-e^{-\Lambda}\right)\left(v_n - q(k)R_n\right)}{C_n R_n \eta(k)\left(1-e^{-\Lambda}\right){V_c}^2(k)} = f(V_c(k),\eta(k),q(k)). \quad (22)$$

It is possible to evaluate the behavior of g as a function of each variable, $V_c(k)$, $\eta(k)$, and $q(k)$. Let's now consider the partial derivatives in (21) (see top of the page). Given that $|q(k)R_n| < v_n$, the sign of the three partial derivatives demonstrates that g decreases when $V_c(k)$, $\eta(k)$, and $q(k)$ increase. As a consequence, the values of g can be evaluated by considering the worst case, corresponding to the highest values of the duty cycle and the quantization noise of the signal to transmit, and the voltage across the ultra-nanocapacitor, i.e., $\eta(k) = T_b/T_s$, $q(k) = \Delta_q/2$, and $V_c(k) = v_n$. The inequality to study is now:

$$g \leq \frac{2v_n T_s - \left(1-e^{-\Lambda}\right)\Delta_q T_s R_n}{C_n R_n T_b \left(1-e^{-\Lambda}\right){v_n}^2}. \quad (23)$$

Given that the minimum acceptable value of the load current is equal to 0 (i.e., the transmission of a frame entirely composed by 0-bits), and its maximum value is $i_{l\,max} = g C_n {v_n}^2 T_b/2T_s$ (i.e., the transmission of a frame composed by only 1-bits when the voltage across the ultra-nanocapacitor is the maximum one), the quantization step size is computed as: $\Delta_q = i_{l\,max}/L = g C_n {v_n}^2 T_b/2LT_s$, where L is the number of quantization levels. The explicit value of Δ_q can be used to solve the aforementioned inequality. The corresponding solution provides a further upper bound for the proportional gain

g, that is $g \leq 4LT_s/R_nC_nv_nT_b\left(1-e^{-\Lambda}\right)(2L+1)$. Furthermore, by considering the initial assumption on the proportional gain g (i.e., $g > 0$), it comes that the sixth condition is satisfied when $0 < g \leq 4LT_s/R_nC_nv_nT_b\left(1-e^{-\Lambda}\right)(2L+1)$. This constraint is used for the calculation of γ_4 in the Theorem.

Finally, the six analyzed conditions must be jointly satisfied. Thus, it is possible to obtain the lower and upper bounds of the proportional gain g, concluding the proof of Theorem 2.

REFERENCES

[1] I. F. Akyildiz, M. Pierobon, and S. Balasubramaniam, "Moving Forward with Molecular Communication: from Theory to Human Health Applications [point of view]," *Proc. IEEE*, vol. 107, no. 5, pp. 858–865, May 2019.

[2] V. Jamali, A. Ahmadzadeh, W. Wicke, A. Noel, and R. Schober, "Channel Modeling for Diffusive Molecular Communication—A Tutorial Review," *Proc. IEEE*, vol. 107, no. 7, pp. 1256–1301, July 2019.

[3] M. Kuscu, E. Dinc, B. Bilgin, H. Ramezani, and O. Akan, "Transmitter and Receiver Architectures for Molecular Communications: A Survey on Physical Design With Modulation, Coding, and Detection Techniques," *Proc. IEEE*, pp. 1–40, 2019.

[4] M. Ş. Kuran, H. B. Yilmaz, T. Tugcu, and B. Özerman, "Energy Model for Communication via Diffusion in Nanonetworks," *Nano Commun. Netw.*, vol. 1, no. 2, pp. 86–95, 2010.

[5] N. Kim and C. Chae, "Novel Modulation Techniques using Isomers as Messenger Molecules for Nano Communication Networks via Diffusion," *IEEE J. Sel. Areas Commun.*, vol. 31, no. 12, pp. 847–856, December 2013.

[6] V. Musa, G. Piro, L. A. Grieco, and G. Boggia, "A Lean Control Theoretic Approach to Energy-Harvesting in Diffusion-Based Molecular Communications," *IEEE Communications Letters*, vol. 24, no. 5, pp. 981–985, 2020.

[7] D. Demiray, A. Cabellos-Aparicio, E. Alarcón, D. T. Altilar, I. Llatser, L. Felicetti, G. Reali, and M. Femminella, "Direct: A Model for Molecular Communication Nanonetworks Based on Discrete Entities," *Nano Commun. Netw.*, vol. 4, no. 4, pp. 181–188, 2013.

[8] J.-T. Huang and C.-H. Lee, "On Capacity Bounds of Two-Way Diffusion Channel with Molecule Harvesting," in *Proc. IEEE ICC*, 2017, pp. 1–6.

[9] H. G. Bafghi, A. Gohari, M. Mirmohseni, G. Aminian, and M. Nasiri-Kenari, "Diffusion-Based Molecular Communication with Limited Molecule Production Rate," *IEEE Trans. Mol. Biol. Multi-Scale Commun.*, 2019.

[10] Y. Deng, W. Guo, A. Noel, A. Nallanathan, and M. Elkashlan, "Enabling Energy Efficient Molecular Communication via Molecule Energy Transfer," *IEEE Commun. Lett.*, vol. 21, no. 2, pp. 254–257, Feb 2017.

[11] W. Guo, Y. Deng, H. B. Yilmaz, N. Farsad, M. Elkashlan, A. Eckford, A. Nallanathan, and C. Chae, "SMIET: Simultaneous Molecular Information and Energy Transfer," *IEEE Wireless Commun.*, vol. 25, no. 1, pp. 106–113, February 2018.

[12] S. Chandrasekaran, C. Bowen, J. Roscow, Y. Zhang, D. K. Dang, E. J. Kim, R. Misra, L. Deng, J. S. Chung, and S. H. Hur, "Micro-Scale to Nano-Scale Generators for Energy Harvesting: Self Powered Piezoelectric, Triboelectric and Hybrid Devices," *Physics Reports*, 2018.

[13] S. Mohrehkesh, M. C. Weigle, and S. K. Das, "Energy Harvesting in Electromagnetic Nanonetworks," *Computer*, vol. 50, no. 2, pp. 59–67, Feb 2017.

[14] J. M. Jornet and I. F. Akyildiz, "Joint Energy Harvesting and Communication Analysis for Perpetual Wireless Nanosensor Networks in the Terahertz Band," *IEEE Trans. Nanotechnol.*, vol. 11, no. 3, pp. 570–580, 2012.

[15] S. Canovas-Carrasco, A.-J. Garcia-Sanchez, and J. Garcia-Haro, "On the Nature of Energy-Feasible Wireless Nanosensor Networks," *Sensors*, vol. 18, no. 5, p. 1356, 2018.

[16] S. A. Wirdatmadja, M. T. Barros, Y. Koucheryavy, J. M. Jornet, and S. Balasubramaniam, "Wireless Optogenetic Nanonetworks for Brain Stimulation: Device Model and Charging Protocols," *IEEE Trans. NanoBiosci.*, vol. 16, no. 8, pp. 859–872, Dec 2017.

[17] M. Donohoe, B. Jennings, J. M. Jornet, and S. Balasubramaniam, "Nanodevice Arrays for Peripheral Nerve Fascicle Activation Using Ultrasound Energy-Harvesting," *IEEE Trans. Nanotechnol.*, vol. 16, no. 6, pp. 919–930, 2017.

[18] H. Khalil, *Nonlinear Systems: Pearson New International Edition*. Always Learning, Pearson Education Limited, 2013.

[19] Z. Cheng, Y. Zhang, and M. Xia, "Performance Analysis of Diffusive Mobile Multiuser Molecular Communication With Drift," *IEEE Transactions on Molecular, Biological and Multi-Scale Communications*, vol. 4, no. 4, pp. 237–247, 2018.

[20] G. H. Alshammri, M. S. Alzaidi, W. K. M. Ahmed, and V. B. Lawrence, "Low-Complexity Memory-Assisted Adaptive-Threshold Detection Scheme for On-Off-Keying Diffusion-Based Molecular Communications," in *Proc. of IEEE Sarnoff Symposium*, Sep. 2017, pp. 1–6.

[21] M. Zoofaghari and H. Arjmandi, "Diffusive Molecular Communication in Biological Cylindrical Environment," *IEEE Trans. NanoBiosci.*, vol. 18, no. 1, pp. 74–83, Jan 2019.

[22] M. Kuscu and O. B. Akan, "Maximum Likelihood Detection With Ligand Receptors for Diffusion-Based Molecular Communications in Internet of Bio-Nano Things," *IEEE Trans. Nanobiosci.*, vol. 17, no. 1, pp. 44–54, Jan 2018.

[23] M. Pierobon and I. F. Akyildiz, "Noise Analysis in Ligand-Binding Reception for Molecular Communication in Nanonetworks," *IEEE Trans. Signal Process.*, vol. 59, no. 9, pp. 4168–4182, 2011.

[24] M. M. Al-Zu'bi and A. S. Mohan, "Modeling of Ligand-Receptor Protein Interaction in Biodegradable Spherical Bounded Biological Micro-Environments," *IEEE Access*, vol. 6, pp. 25 007–25 018, 2018.

[25] M. U. Mahfuz, D. Makrakis, and H. T. Mouftah, "A Comprehensive Study of Sampling-Based Optimum Signal Detection in Concentration-Encoded Molecular Communication," *IEEE Trans. NanoBiosci.*, vol. 13, no. 3, pp. 208–222, Sep. 2014.

[26] M. Mukherjee, H. B. Yilmaz, B. Bhowmik, J. Lloret, and Y. Lv, "Synchronization for Diffusion-Based Molecular Communication Systems via Faster Molecules," in *Proc. IEEE ICC*, May 2019, pp. 1–5.

[27] H. ShahMohammadian, G. G. Messier, and S. Magierowski, "Blind Synchronization in Diffusion-Based Molecular Communication Channels," *IEEE Commun. Lett.*, vol. 17, no. 11, pp. 2156–2159, November 2013.

[28] C. Gonzalez-Solino and M. D. Lorenzo, "Enzymatic Fuel Cells: Towards Self-Powered Implantable and Wearable Diagnostics," *Biosensors*, vol. 8, no. 1, p. 11, 2018.

[29] W. Jia, G. Valdés-Ramírez, A. J. Bandodkar, J. R. Windmiller, and J. Wang, "Epidermal Biofuel Cells: Energy Harvesting from Human Perspiration," *Angewandte Chemie International Edition*, vol. 52, no. 28, pp. 7233–7236, 2013.

[30] I. Ivan, T. Vidaković-Koch, and K. Sundmacher, "Recent Advances in Enzymatic Fuel Cells: Experiments and Modeling," *Energies*, vol. 3, April 2010.

[31] S. Xu, Y. Qin, C. Xu, Y. Wei, R. Yang, and Z. L. Wang, "Self-Powered Nanowire Devices," *Nature nanotechnol.*, vol. 5, no. 5, p. 366, 2010.

[32] Z. L. Wang, X. Wang, J. Song, J. Liu, and Y. Gao, "Piezoelectric Nanogenerators for Self-Powered Nanodevices," *IEEE Pervasive Computing*, vol. 7, no. 1, pp. 49–55, Jan 2008.

[33] J. Briscoe, N. Jalali, P. Woolliams, M. Stewart, P. M. Weaver, M. Cain, and S. Dunn, "Measurement Techniques for Piezoelectric Nanogenerators," *Energy & Environmental Science*, vol. 6, no. 10, pp. 3035–3045, 2013.

[34] Z. L. Wang and J. Song, "Piezoelectric Nanogenerators based on Zinc Oxide Nanowire Arrays," *Science*, vol. 312, no. 5771, pp. 242–246, 2006.

[35] X. Wang, "Piezoelectric Nanogenerators—Harvesting Ambient Mechanical Energy at the Nanometer Scale," *Nano Energy*, vol. 1, no. 1, pp. 13–24, 2012.

[36] B. Saravanakumar, R. Mohan, K. Thiyagarajan, and S.-J. Kim, "Fabrication of a ZnO Nanogenerator for Eco-Friendly Biomechanical Energy Harvesting," *RSC Advances*, vol. 3, no. 37, pp. 16 646–16 656, 2013.

[37] S. Xu, B. Hansen, and Z. Wang, "Piezoelectric-Nanowire-Enabled Power Source for Driving Wireless Microelectronics," *Nature commun.*, vol. 1, p. 93, 2010.

[38] X. Niu, W. Jia, S. Qian, J. Zhu, J. Zhang, X. Hou, J. Mu, W. Geng, J. Cho, J. He *et al.*, "High-Performance PZT-Based Stretchable Piezoelectric Nanogenerator," *ACS Sustainable Chemistry & Engineering*, vol. 7, no. 1, pp. 979–985, 2018.

[39] L. Wei, Q.-X. Liu, B. Zhu, W.-J. Liu, S.-J. Ding, L. Hong, A. Jiang, and D. Zhang, "Low-Cost and High-Productivity Three-Dimensional Nanocapacitors Based on Stand-Up ZnO Nanowires for Energy Storage," *Nanoscale research lett.*, vol. 11, p. 213, Dec 2016.

[40] D. Pech, M. Brunet, H. Durou, P. Huang, V. Mochalin, Y. Gogotsi, P.-L. Taberna, and P. Simon, "Ultrahigh-Power Micrometre-Sized Supercapacitors Based on Onion-Like Carbon," *Nature nanotechnol.*, vol. 5, no. 9, p. 651, 2010.

[41] S. P. Badwal, S. S. Giddey, C. Munnings, A. I. Bhatt, and A. F. Hollenkamp, "Emerging Electrochemical Energy Conversion and Storage Technologies," *Frontiers in chemistry*, vol. 2, p. 79, 2014.

[42] R. A. Freitas, *Nanomedicine, Volume I: Basic Capabilities*, 1st ed. Landes Bioscience, 1999.
[43] N. Farsad, W. Guo, and A. W. Eckford, "Tabletop Molecular Communication: Text Messages Through Chemical Signals," *PloS one*, vol. 8, no. 12, p. e82935, 2013.
[44] Y. Y. Chen, "Nano-Scale Control Design and Its' Practical Implementation of Piezoelectric Materials," in *Advanced Materials Research*, vol. 939. Trans Tech Publ, 2014, pp. 663–670.
[45] K. Iniewski, *Circuits at the nanoscale: communications, imaging, and sensing*. CRC Press, 2018.

Vittoria Musa (Student Member, IEEE) received the B. Sc. and M.Sc. degrees (both with honors) in telecommunication engineering from Politecnico di Bari, Bari, Italy, in 2016 and 2018, respectively. She is currently pursuing the Ph.D. degree with the Department of Electrical and Information Engineering at the Politecnico di Bari. Her main research interests include nano-networks, nanoscale wireless communications at the terahertz band, and molecular communications.

Giuseppe Piro (Member, IEEE) Since November 2018, he is an Assistant Professor in Telecommunication at Politecnico di Bari. In March 2018, he held the habilitation as "Associate Professor" in Telecommunications Engineering, according to the National Scientific Habilitation procedure (ASN 2016-2018). He received a first level degree and a second level degree (both cum laude) in Telecommunications Engineering from "Politecnico di Bari", Italy, in 2006 and 2008, respectively. He received the Ph.D. degree in Electronic Engineering from "Politecnico di Bari", Italy, on March 2012. His main research interests include secure Internet of Things and Industry 4.0, 5G systems, data-centric and programmable architectures for the Future Internet, nano-networks, Internet models and network measurements. His research activity is documented in more than 80 peer-reviewed international journals and conference papers, accounting for more than 3800 citations and a H-index of 24 (Scholar Google). At the time of this writing, he is the local investigator of the PRIN project no. 2017NS9FEY entitled "Realtime Control of 5G Wireless Networks: Taming the Complexity of Future Transmission and Computation Challenges". Moreover, he is involved in the European EU H2020 GUARD project. He is also involved in Italian MIUR PON projects (Pico&Pro, FURTHER, AGREED, RAFAEL) and in Apulia Region (Italy) Research project INTENTO. He founded 5G-ai-simulator, LTE-Sim, and NANO-SIM projects and is a developer of Network Simulator 3. In the past, he was involved in EU H2020 projects, like FANTASTIC-5G, BONVOYAGE, and symbIoTe, as well as in the "Apulia Israel joint Accelerator (AIJA)" project. He is also regularly involved as member of the TPC of many prestigious international conferences. Currently, he serves as Associate Editor for Sensors journal (MDPI), Internet Technology Letter (Wiley) and Wireless Communications and Mobile Computing journal (Hindawi).

L. Alfredo Grieco (Senior Member, IEEE) received the Dr. Eng. degree (with honors) in electronic engineering from "Politecnico di Bari," Bari, Italy, in Oct. 1999 and the Ph.D. degree in information engineering from "Università di Lecce," Lecce, Italy, on December 2003. From Jan. 2005 to Oct. 2014, he held an Assistant Prof. position at the "DEI - Politecnico di Bari". From March to June 2009, he has been a Visiting Researcher with INRIA (Sophia Antipolis, France), working on the topic of Internet measurements. From Oct. to Nov. 2013, he has been a Visiting Researcher with LAAS-CNRS (Toulouse, France) working on Information Centric Networking design of M2M systems. From Nov. 2014 to Dec. 2018, he has been an Associate Professor in Telecommunications at Politecnico di Bari (DEI). Since Dec. 2018, he is a Full Professor in Telecommunications at Politecnico di Bari (DEI). He authored around 200 scientific papers published in venues of great renown that gained more than 8000 citations. His current research interests include: Industrial Internet of Things, Information Centric Networking, and Nano-communications. He is the Founder Editor in Chief of the Internet Technology Letters Journal (Wiley) and served as EiC of the Transactions on Emerging Telecommunications Technologies (Wiley) from mid-2016 to 2019. He also serves as associate editor the IEEE Transactions on Vehicular Technology journal (for which he has been awarded as top associate editor in 2012 and 2017). He has been constantly involved as Technical Program Committee member of many prestigious conferences. Within the Internet Engineering Task Force (Internet Research Task Force), he contributed (as author of RFC 7554) new standard protocols for industrial IoT applications (new standard architectures for tomorrow ICN-IoT systems). From Jan. 2019, he is Founding Member and Subarea-Chair of the IEEE SIG on Intelligent Internet Edge. In 2020 he has been nominated scientific coordinator of the IoT4.0 Lab.

Gennaro Boggia (Senior Member, IEEE) received, with honors, the Dr. Eng. and Ph.D. degrees in electronics engineering, both from the Politecnico di Bari, Bari, Italy, in July 1997 and March 2001, respectively. Since September 2002, he has been with the Department of Electrical and Information Engineering, Politecnico di Bari, where he is currently a Full Professor. From May 1999 to December 1999, he was a Visiting Researcher with the TILab, TelecomItalia Lab, Torino, Italy, where he was involved in the study of the core network for the evolution of Third-Generation (3G) cellular systems. In 2007, he was a Visiting Researcher at FTW, Vienna, Austria, where he was involved in activities on passive and active traffic monitoring in 3G networks. He has authored or coauthored more than 150 papers in international journals or conference proceedings, gaining more than 2300 citations. He is active in the IETF ICNRG working group and in the IEEE WG 6TiSCH. He is also regularly involved as a Member of the Technical Program Committee of many prestigious international conferences. His research interests include the fields of Wireless Networking, Cellular Communication, Internet of Things (IoT), Network Security, Security in Iot, Information Centric Networking (ICN), Protocol stacks for industrial applications, Internet measurements, and Network Performance Evaluation. Dr. Boggia is currently an Associate Editor for the IEEE Commun. Mag., the ETT Wiley Journal, and the Springer Wireless Networks journal.